



HAL
open science

Fast Nonlinear Method for Static Aeroelasticity Applied to High Aspect Ratio Wings

Oriol Chandre-Vila, Jean-Philippe Boin, Bernard Barriety, Yann Nivet,
Joseph Morlier, Nicolas Gourdain

► **To cite this version:**

Oriol Chandre-Vila, Jean-Philippe Boin, Bernard Barriety, Yann Nivet, Joseph Morlier, et al.. Fast Nonlinear Method for Static Aeroelasticity Applied to High Aspect Ratio Wings. *Journal of Aircraft*, 2023, pp.1-21. 10.2514/1.C037052 . hal-03985408

HAL Id: hal-03985408

<https://hal.science/hal-03985408>

Submitted on 14 Feb 2023

HAL is a multi-disciplinary open access archive for the deposit and dissemination of scientific research documents, whether they are published or not. The documents may come from teaching and research institutions in France or abroad, or from public or private research centers.

L'archive ouverte pluridisciplinaire **HAL**, est destinée au dépôt et à la diffusion de documents scientifiques de niveau recherche, publiés ou non, émanant des établissements d'enseignement et de recherche français ou étrangers, des laboratoires publics ou privés.

Fast Nonlinear Method for Static Aeroelasticity Applied to High Aspect Ratio Wings

Oriol Chandre-Vila* and Jean-Philippe Boin[†] and Bernard Barriety[‡] and Yann Nivet[§]
AIRBUS OPERATIONS SAS, 316 Route de Bayonne, 31060 Toulouse, France.

Joseph Morlier[¶]
*ICA, Université de Toulouse, ISAE-SUPAERO, MINES ALBI, UPS, INSA, CNRS
3 Rue Caroline Aigle, 31400 Toulouse, France.*

Nicolas Gourdain^{||}
ISAE-SUPAERO, 10 Avenue Edouard Belin, 31055 Toulouse

A fast methodology for steady-state nonlinear aeroelastic calculations across a range of Mach regimes is developed for wings with high aspect ratio, where flexible behaviors are experienced. The methodology recovers the pressure field from a high-fidelity database using the local incidence estimated with a Vortex Lattice Method. Investigations are performed at different Mach regimes (sub- and transonic) for a XRF1 High Aspect Ratio Wing. CFD/CSM results are used to compare the flexible FNSA (*Fast Nonlinear Static Aeroelasticity*) method. Overall accurate results are obtained for both configurations, reducing the computation time from seven and a half hours (CFD) to one second (FNSA).

I. Nomenclature

b	=	semi wingspan
c	=	chord
Ca	=	cant angle
C_d	=	drag coefficient
C_l	=	lift coefficient
C_m	=	pitching moment coefficient
C_p	=	pressure coefficient
M	=	Mach number
M_∞	=	freestream Mach number

*PhD Candidate, Department of Loads & Aeroelasticity, oriol.chandre-vila@airbus.com, oriol.chandre-vila@isae-supaero.fr.

[†]Loads & Aeroelastics Engineer, Department of Loads & Aeroelasticity, jean-philippe.boin@airbus.com.

[‡]Loads & Aeroelastics Engineer, Department of Loads & Aeroelasticity, bernard.barriety@airbus.com.

[§]Loads & Aeroelastics Engineer, Department of Loads & Aeroelasticity, yann.nivet@airbus.com.

[¶]Professor, AIAA Member, Department of Mechanics, Structures and Materials, joseph.morlier@isae-supaero.fr.

^{||}Professor, Department of Aerodynamics, Energetics and Propulsion, nicolas.gourdain@isae-supaero.fr.

N_s	=	spanwise divisions
n_y	=	Y-component of the local normal vector
n_z	=	Z-component of the local normal vector
Q	=	VLM AIC matrix
R_y	=	rotation along Y-axis
R_z	=	rotation along Z-axis
T_z	=	translation along Z-axis
α , AoA	=	angle of attack
β	=	sideslip angle
δ	=	dihedral angle
η	=	dimensionless wingspan
λ	=	Prandtl-Glauert compressibility correction
ϕ	=	structural twist angle
φ	=	structural sweep angle
$\frac{\partial C_l}{\partial \alpha}$	=	lift slope
$\Delta\alpha_{flex}$	=	local delta incidence due to flexibility
$\Delta\beta_{flex}$	=	local delta sideslip due to flexibility

II. Introduction

In the inherent evolution of aircraft design, cutting edge investigations are focused on improving the flight performance. Designing the wing is a key player in the aerodynamic efficiency of the airplane. Aircraft manufacturers find stimulating to design it slenderer to benefit from a lighter flexible wing. Just to give an example, this advantageous behavior permits to achieve a reliable stiffness with no extra reinforcement [1][2][3]. Furthermore, airflow could be diverted thanks to the higher surface area of a fully flexible wing using the energy available in the airflow to improve the performance whereas requiring fewer moving parts for controlling the flight [4] or to take advantage of the structural deformations to enhance performance and to alleviate loads [5][6].

As a consequence of this augmentation of flexibility, the interconnection of different disciplines is permanently present. The flexible structure affects the shape of the wing, thus the aerodynamic field changes and so do the air forces which consequently re-affect the structure, and so forth. When this phenomena is studied together with the aircraft maneuverability, control laws play an important role and the difficulty of the study augments considerably. Thus, another field of study in the aircraft industry is MDO problems [7][8], yielding to designs which consider a wider range

of physics phenomena from different nature.

In order to keep the computation time of Multidisciplinary Design Optimization (MDO) competitive, fast methodologies for each individual discipline need to be implemented. Thus, the capacity of a single solver to capture different phenomena in a highly competitive time has an enormous transcendence in the global MDO process [9]. Moreover, when treating MDO in a pre-design phase, a fast methodology permits to analyze more possible solutions [10][11][12].

In the context of aeroelasticity [13] such a solution has a direct impact on the design of control surfaces from the beginning of the conceptual phase [14]. For some years now, new methodologies have been adapted to nonlinear, as well as unsteady, studies in order to quickly solve the problem. These different methodologies can rely in several levels of fidelity [15][16]. Crovato et al. in [17] assessed the impact of the aerodynamic level of fidelity used in preliminary aircraft design concluding that a nonlinear method is required to reliably perform steady aerodynamic computations on rigid wings.

Aircrafts flying at high subsonic or transonic speeds during cruise can experience different types of nonlinearities. In static aeroelasticity, the nature of these nonlinearities can be identified as structural or aerodynamic. In Table 1 the different hypothesis about how to face these phenomena are exposed.

While different aerodynamic methodologies exist for a fast treatment of the problem (Vortex Lattice Method (VLM) [20] or Prandtl's lifting line [21], among others), very few of them are able to capture both aerodynamic nonlinearities. These fast solutions are based on the potential theory and have a simple approach for the effects of the 3D (finite) wing [22][23].

The capabilities of these fast solvers are empowered by enriching the data with high-fidelity solutions [24]. The final solver benefits from the low computational demand and the three dimensional treatment of the VLM. In detail, the effective incidence seen by each section in span is decomposed into a global incidence, a twist effect and an induced incidence, due to 3D aerodynamic effects. The latest effect is calculated using an iterative coupling between prediction of the lifting surface and of the viscous method; allowing to retrieve the three dimensional aerodynamics for a given twist. Then, complementing the solver with high accurate expensive computations, the resultant methodology is capable of capturing both kinds of aerodynamic nonlinearities.

Grozdanov et al. presented a methodology based on the above-mentioned principles in [25]. In there, a nonlinear vortex-lattice method coupled with 2D transonic Computational Fluid Dynamics (CFD) solutions is examined and, adding a finite element beam model, it is found to be an inexpensive solution capable of predicting the aeroelastic wing

Table 1 Synthesis of the possible nonlinearities identified in static fluid-structure interaction problem. [18][19].

STRUCTURAL	Unique Reference Shape	Flexibility effects are taken into account through linear local incidence change, but the unique reference shape is used for integration.
	Geometric Linear Effect	Linear deformed shape is used, thus it changes due to the deformation and the linear local incidence. Used when the deformation due to bending moment is less than 10% semi-span. The wing is artificially enlarged in order to respect the deformed shape and the initial span.
	Geometric Non-linear Effect	Nonlinear deformed shape is used, thus it changes due to the deformation and the nonlinear local incidence. Used when the deformation due to bending moment is high and the span reduction is higher than 10%. The wing preserve the span and the deformed shape.
	Nonlinear Stiffness	Besides of the geometric nonlinear effect characteristics, nonlinear behavior of the structure's stiffness is treated. It is needed a nonlinear FEM.
AERODYNAMICS	Incidence Nonlinearity	Characterized by a stall that originates due to the angle seen by the airfoil when the freestream impacts the wing.
	Transonic Nonlinearity	Instabilities that originates under local sonic conditions. The freestream velocity is high, but not necessarily sonic or supersonic. The shock waves are not fixed.

behavior in the transonic regime. Goitia et al. in [26] presented the capabilities of a 2.5D methodology in capturing the stall behavior of an empennage comparing its results to CFD and Wing Tunnel Test (WTT). Kontogiannis et al. presented in [27] the potential of the method capturing the wing-body effects by upgrading the potential VLM to a panel formulation.

Skujins et al. [28] adapted a similar concept to suitably capture unsteady effects for a hypersonic vehicle in a wide range of Mach numbers. This solution merges the fast methodology with a Reduced Order Model (ROM) for storing the data. The real time simulation remains greatly competitive both in time and computation cost. The problem normally needs to be reformulated in order to efficiently implement a ROM solution, used by a considerable amount of methodologies. For instance, Bekemeyer et al. in [29] compare an unsteady nonlinear ROM based on least-squares residual minimization to the linearised frequency-domain method. And, Rule et al. in [30] propose an aerodynamic ROM based on the balanced truncation.

Barriety et al. in [31] achieve it with only one step whereas other solutions normally need two steps to calculate the incidence variation (first the effect of the structural deformation to the aerodynamic and then the induced effects

variations of the deformation). Then, this local delta incidence computed by a VLM is enriched with high-fidelity data (WTT, CFD or flight data). Condensed aerodynamics are used to recover local C_l and C_m and, defied against WTT and CFD/CSM (Computational Fluid Dynamics/Computational Structure Mechanics) calculations, the method shows to be rapid, robust, and, to be capable of capturing the aerodynamic nonlinearities.

The current paper tackles an extension of the methodology introduced by Barriety et al. applied in a flexible academic wing –the XRF1 High Aspect Ratio Wing [32] [33]– for several Mach numbers. This extension works is able to treat local pressures, yielding to a wide post-process uses (from handling qualities to local loads analysis). The fast method solutions are compared to high-fidelity CFD/CSM results.

Furthermore, in order to capture the lateral effect induced by dihedral angle or a winglet, a delta of sideslip angle (β) has been introduced following the same principles as in the delta of incidence (α). Furthermore, in order to enhance the precision, the structural nonlinear treatment has been updated to increase the accuracy of the method –in particular drag and moment loads.

The final goal of this paper is, though, to demonstrate the capacity of the proposed methodology to reproduce the aerodynamic behavior for a wide range of Mach regimes (below sonic conditions) when the flexibility strongly affects the performance. And we also ambition to demonstrate that the methodology is highly robust and fast.

This work first presents the high-fidelity solvers characteristics in section III. A mesh convergence shows the reliability of the mesh. A turbulence study is also performed. Besides, the effect of flexible wing into the Aerodynamics is presented. Then, in section IV, the new formulation for the fast methodology proposed is presented. Above all, the theoretical formulation and its implementation using a VLM approach. Moreover, in section V, the performance of the method is evaluated for the cruise Mach, the C_p at the winglet is analyzed, the performance at different Mach regimes is evaluated and, to complete with study of the new fast formulation, the sensibility to the mesh VLM is analyzed.

III. Aeroelastic analysis using high-fidelity methods

In this project two high-fidelity processes have been run using a computer with 2 CPU and 8 GB. On one hand, for the lookup tables creation, CFD simulations have been computed for different Mach numbers each 0.1° . On the other hand, the flexible FNSA is faced to CFD/CSM simulations, where aerodynamic and structural solvers are coupled. The mechanics computation is solved with Nastran using Linear Static Analysis (Solution 101) [34]. The output data available consist of displacements, grid point loads, elements forces and stresses, and support reactions. Then, fluid dynamics solver uses the CFD code TAU [35].

A. Mesh analysis

In order to validate the aerodynamic process, two studies have been performed: one for the mesh convergence, and another one for the turbulence model convergence.

Firstly, a coarse mesh is faced to a fine mesh 4.6 times smoother. In Fig. 1, polar curves for different Mach regimes are presented. It is verified that the difference in the mesh size does not imply an error in our calculations. As matter of fact, the maximum differences between both cell-sizes are seen in $M = 0.85$ (2.57% for C_l , 3.16% for C_d and 8.93% for C_m) and in the others, the differences remain almost negligible (except for an error of 4.04% for C_m at $M = 0.50$). Appreciable differences appear just in the transonic regime when computing C_m . For the other two coefficients, the two different qualities of mesh offers the same performance.

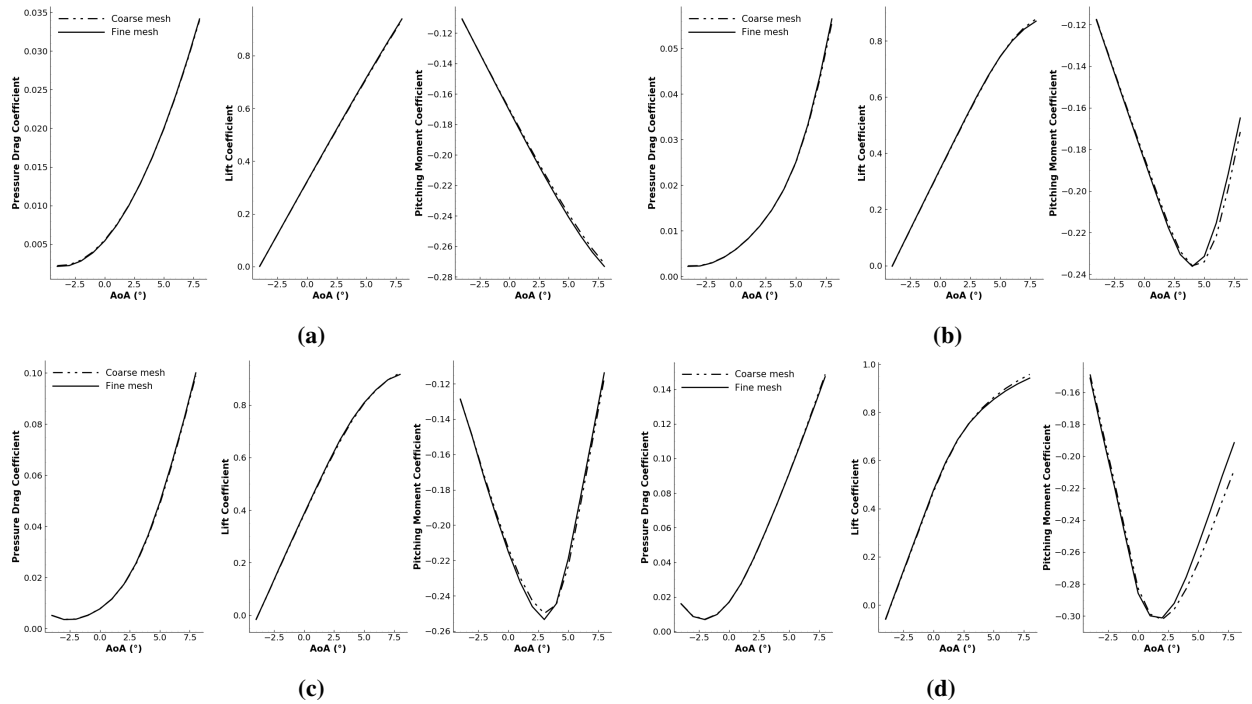


Fig. 1 Mesh size convergence: polar curves between coarse and fine mesh results. (a) $M = 0.30$, (b) $M = 0.50$, (c) $M = 0.70$ and, (d) $M = 0.85$.

Once the mesh has been evaluated, the coarse mesh is used to perform a turbulence model analysis. The first model considered is the one-equation Spalart-Allmaras approach which is based in a transport equation for a viscosity-like variable ($\tilde{\nu}$) in order to compute the kinematic eddy viscosity (ν_T) [36]. The second model is the Wilcox SST $k - \omega$ which is a combination of formulation $k - \omega$ and $k - \varepsilon$ to ensure the best performance. It uses two transportation equations, one for the turbulent kinetic energy (k) and another for the specific dissipation rate (ω) [37]. Then, the last and third model considered is the Reynolds Stress Models (RSM) which avoids the eddy viscosity by calculating the individual components of the Reynolds stress tensor resulting of the solved transport equation [38].

In Fig. 2, the results for the CFD simulations prove that the effect of the turbulence model has a higher impact when

simulating high Mach regimes and, with the results presented, RSM model of turbulence is selected because a better general performance is achieved. For convergence, the residual is wanted to be below 10^{-5} .

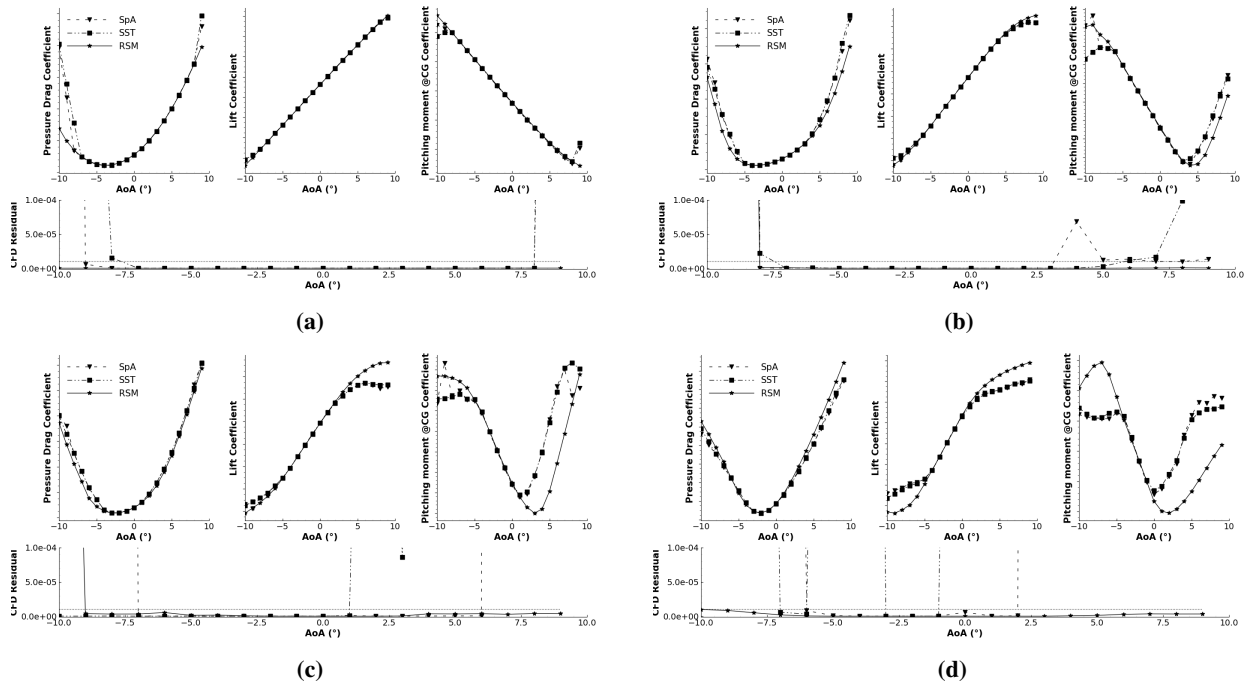


Fig. 2 Turbulence analysis for the CFD simulation. (a) $M = 0.30$, (b) $M = 0.50$, (c) $M = 0.70$, (d) $M = 0.85$.

B. High-fidelity results

The goal in this work is to evaluate our FNSA within a flexible aircraft wing test case. Thus, it is necessary to ensure that deformations of the selected wing are significant to appreciate differences between its flexible and its rigid behavior. With this aim, a CFD/CSM study has been conducted for a transonic cruise Mach number ($M = 0.83$), at a similar incidence as the one expected in a cruise regime ($\alpha = 2^\circ$). The case deformations are presented in Fig. 3. The selected wing responds to the requirements of flexibility since it reaches near $0.11b$ of vertical displacement.

The last aspect analyzed in these previous results is the effect of flexibility in the pressure field. With that purpose, the C_p at $\alpha = 7^\circ$ is compared together with the pressure field for both cases (rigid and flexible) and they are presented in Fig. 4. The results are shown for a spanwise section $\eta = 0.95$. The deformation experienced by the wing influences the section by easing the aerodynamic load in the leading edge. On one hand, a pronounced depression is noted in the front region of the rigid airfoil. On the other hand, a flatter pressure coefficient is identified for the upper surface of the flexible airfoil. This difference leads to the alleviation of loads: the profile is more uniformly charged along the chord what reduces the leading edge force and, thus, the pitching moment of the section changes.

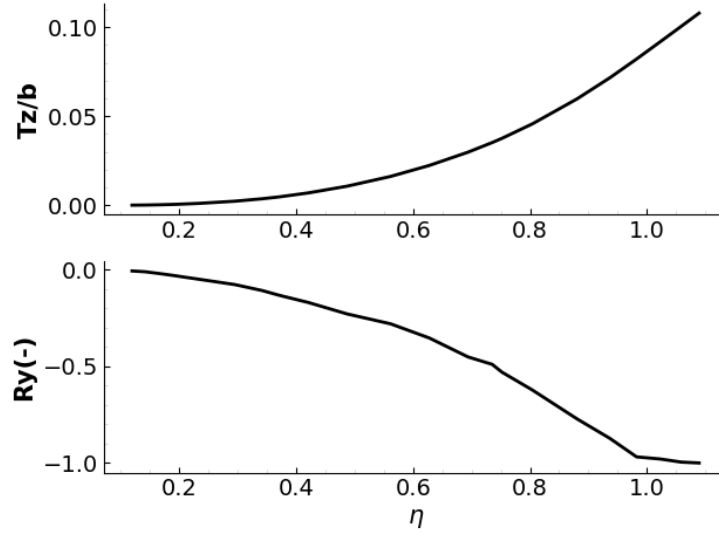


Fig. 3 Structural deformations (Tz/b) (vertical displacement) and (Ry) (twist; made dimensionless by dividing each value by the maximum torsion deformation angle) for $M = 0.83$ and $\alpha = 2^\circ$.

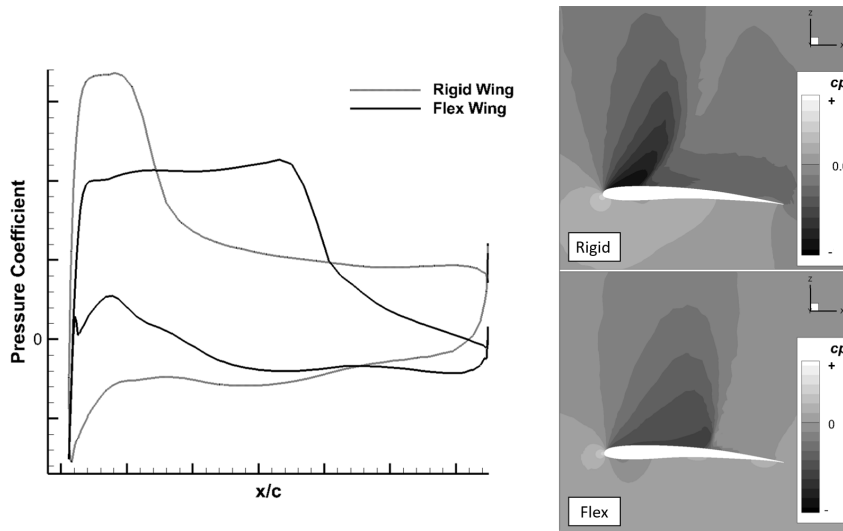


Fig. 4 C_p comparison together with the pressure field for $M = 0.83$ and $\alpha = 7^\circ$ at $\eta = 0.95$.

IV. Formulation

A. Theoretical background

Clearly, the flexible behavior of the wing has an influence in the aerodynamic performance. In Fig. 5, a schematic local lift coefficient for two rigid-wing profile are presented. The difference between both shapes is a different twisting law in the wing.

When considering a point in the B-wing airfoil curve from Fig. 5, we find a different C_l for the same incidence and a different α to create the same lift coefficient. We identify these differences as ΔC_l and $\Delta\alpha$, respectively. Furthermore,

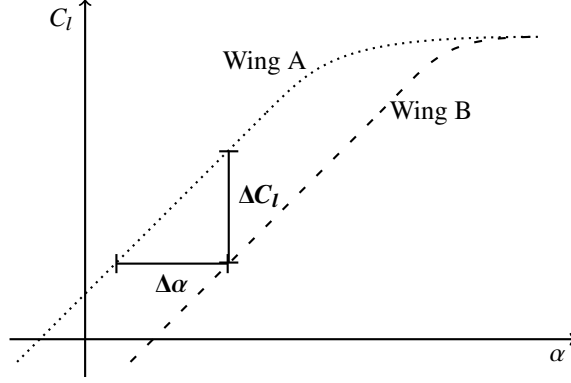


Fig. 5 Schematic C_l v. α graph for two rigid-wing profiles. $\Delta\alpha$ refers to the variation of incidence necessary to obtain the same lift coefficient with the two behaviors. ΔC_l refers to the difference of lift coefficient for the same incidence.

we can approximate the gradient (lift slope) of both rigid curves as:

$$\left(\frac{\partial C_l}{\partial \alpha}\right)_{rigid} \approx \frac{\Delta C_l}{\Delta \alpha} \quad (1)$$

Consistently to Fig. 5, ΔC_l could generally be identified as the product of the AIC matrix by the difference between both twisting laws:

$$\Delta C_l = AIC \cdot [\phi_A - \phi_B] \quad (2)$$

Then, the gradient of the curve is expressed by terms of the AIC matrix, the unitary downwash vector ($\{w_j\} = \{1\}$) and the dihedral:

$$\frac{\partial C_l}{\partial \alpha} = AIC \cdot \{1\} \cdot \cos \delta \quad (3)$$

In Fig. 6, the dihedral angle and the winglet cant angle are identified. Figure 5 refers to a local section of the wing and δ in Eq. (3) is the dihedral angle of the mesh cell. So, $\cos \delta$ locally defined equals to the Y-component of the local normal vector (\mathbf{n}_y). Thus, this formulation recognizes directly the presence of any geometry (i.e. nonconstant dihedral, winglet or vertical tail plane).

Introducing Eq. (2) and (3) to Eq. (1):

$$\Delta \alpha = \frac{AIC \cdot [\phi_A - \phi_B]}{AIC \cdot \{1\} \cdot \cos \delta} = \frac{AIC \cdot R_y}{AIC \cdot \{1\} \cdot \cos \delta} \quad (4)$$

Barriety et. al. in [31] supports the formulation developed from Fig. 5 with WTT results. They concluded that calculating it in the linear region and considering it constant for all incidences (for the same section) is physically loyal to the practical results.

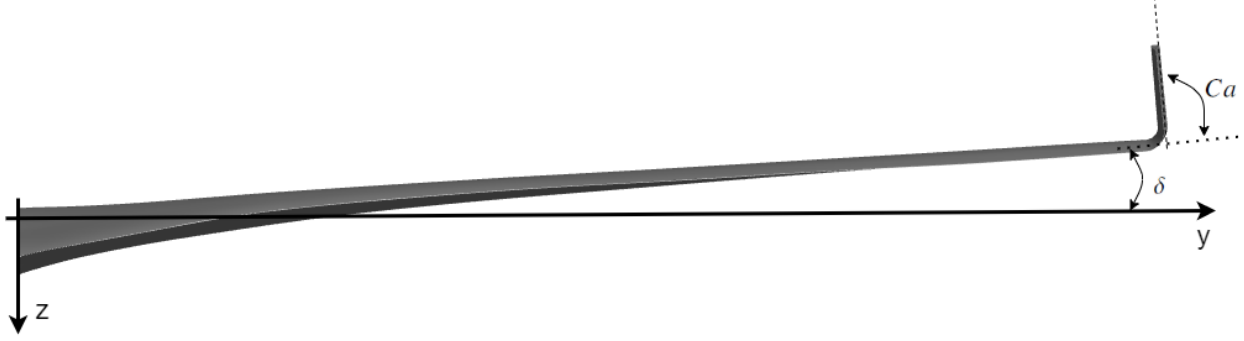


Fig. 6 Scheme of the wing dihedral angle δ (angle between the XY-plane and the wing) and cant angle Ca (angle between wing and winglet planes).

When components such as the VTP or winglet exist, the XZ-plane becomes important; thus, the sideslip angle (β) can be seen as the directional angle of attack. Whether in α the twist is important, here it is the structural sweep angle. Similarly, the gradient with respect to β is driven by the sine, hence the Z-component of the local normal vector (\mathbf{n}_z). So, the equivalent of the Eq. (4) for the sideslip is:

$$\Delta\beta = \frac{AIC \cdot [\varphi_A - \varphi_B]}{AIC \cdot \{1\} \cdot \sin \delta} = \frac{AIC \cdot R_z}{AIC \cdot \{1\} \cdot \sin \delta} \quad (5)$$

A really important benefit of the proposed formulation is the capacity to compute in just one step the influence of the structural deformation and its induced effects. Our $\Delta\alpha$ in Eq. (4) is the $\Delta\alpha_{eff}$ presented in Fig. 7.

B. VLM formulation

From the theoretical expressions of Eq. (4) and (5), the process is able to compute (locally) a new rigid shape from a known one and the difference in twisting between both. Furthermore, it is assumed that the local flexible pressure field will match a rigid one for the corresponding Mach and efficient incidence (updated using structural deformation). Thus, for constructing a flexible solution for a specific incidence, it is needed to travel strip by strip the whole wing, computing at every section the *new* twisting law and saving the corresponding rigid information. In order to do this sectional treatment, a strip summation matrix (S) needs to be introduced in our formulation.

In order to compute the right local twisting that permits to recover the equivalent flexible behavior, a VLM approach is used yielding to Eq. (6) and (7). Since the input of these equations are the structural deformations and the output is a aerodynamic incidence, an interpolation matrix (IM) is required to link the structural grid to the aerodynamic nodes and to orientate the strip using the normal vector. Then, identifying Q as the AIC matrices, the difference of the angles

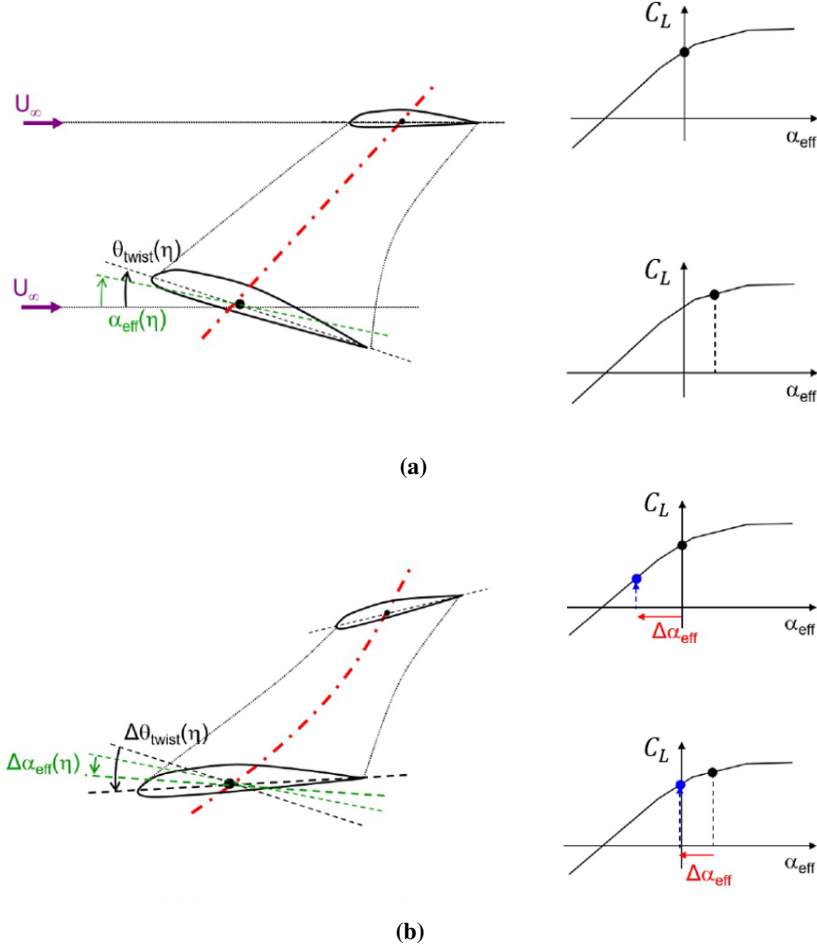


Fig. 7 Local angles dissection: (a) For the initial wing configuration, the local effective total angle of attack is the sum of the geometric alpha, the twist and the induced angle: $\alpha_{eff}(\eta) = \alpha_{geo} + \theta(\eta) + \alpha_{ind}(\eta)$, (b) For the deformed wing (or a second twisting law): $\Delta\alpha_{eff}(\eta) = \Delta\theta(\eta) + \Delta\alpha_{ind}(\eta)$

due to flexibility at each section is:

$$\Delta\alpha_{flex}(\eta) = \frac{S \cdot (Q \cdot IM)}{S \cdot (Q \cdot \mathbf{n}_y)} \cdot R_y \quad (6)$$

$$\Delta\beta_{flex}(\eta) = \frac{S \cdot (Q \cdot IM)}{S \cdot (Q \cdot \mathbf{n}_z)} \cdot R_z \quad (7)$$

Equations (6) and (7) expressed mathematically what Fig. 8 shows graphically: the 3D effects yield to a $\Delta\alpha_{flex} \neq 0$ at the wing root and to:

$$\Delta\alpha_{flex}(\eta) \neq R_y(\eta) \quad \Delta\beta_{flex}(\eta) \neq R_z(\eta) \quad (8)$$

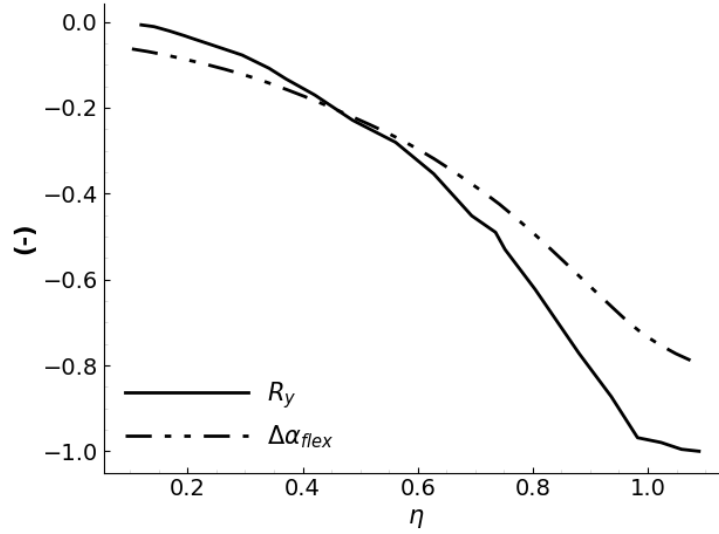


Fig. 8 Local R_y and $\Delta\alpha_{flex}$ (both dimensionless) at $M = 0.83$ and $AoA = 2^\circ$.

C. Compressibility treatment

A challenge when treating a wide range of Mach numbers (highly important in transonic regimes) is the definition of a method that yields to accurate results whereas remaining simple and robust. To that purpose, Prandtl–Glauert is implemented [39]. It is found by linearizing the potential equations associated with compressible, inviscid flow. The principle behind it is to divide the incompressible flow parameter by a factor depending on the freestream Mach number (M_∞) to estimate the contribution of transonic effects to the performance:

$$\lambda = \sqrt{|1 - M_\infty^2|} \quad (9)$$

This correction is introduced into the calculation by adapting the longitudinal coordinate $x' = x/\lambda$.

D. Fast Nonlinear Static Aeroelasticity (FNSA)

With FNSA we can perform three types of analysis: *(a)* a rigid case where only the aerodynamic database is introduced and treated, *(b)* a flexible case where the deformation is imposed to compute the flexible pressure field (used for this aerodynamic model validation work), and, *(c)*, an aeroelastic case where the coupling is performed within flexible FNSA (see Fig. 10).

For these computations, a VLM grid allows the introduction of 3D effects. Equations (6) and (7) link this grid to the structural grid (G1 set); thus, the fluid-structure interaction is coupled (see Fig. 9). However, the organization of the data stored in the lookup tables depends on the data provenance. In our study, a CFD grid resembles the local coefficient of pressure.

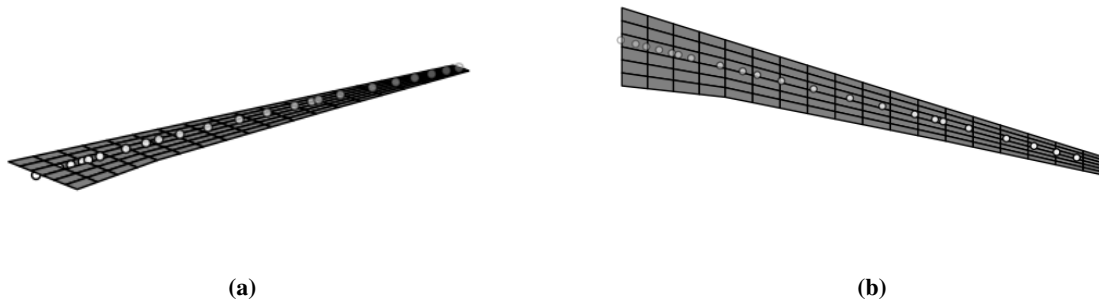


Fig. 9 Structural and Aerodynamic discretization used in the FNSA: the round points are the G1set, while the grid is the VLM mesh (for this illustration, 20 spanwise panels for 8 chordwise are used). (a) isometric view, (b) top view.

Two observations from the static aeroelastic loop (see Fig. 10) are interesting. Firstly, as it has been detailed before, the set of the lookup tables can be loaded from CFD simulation data, from WTT or from a flight test campaign. This capability of empowering the results using different data gives to the method an inherent robustness without a lost in speed. This database is classified by α , β , Mach number and wingspan position (η).

Secondly, the structural model is a condensed stiffness model which represent the wing as a simple line of nodes (beam approach). The condensed stiffness model is clamped (usually in the centre wing-box area) and a flexibility matrix is calculated.

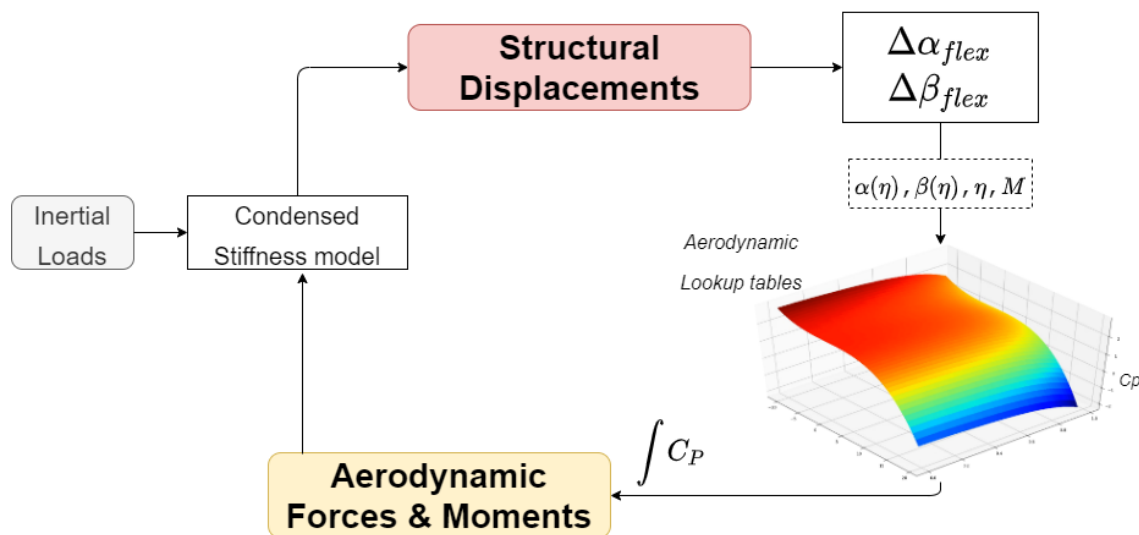


Fig. 10 Fast Nonlinear Static Aeroelasticity scheme.

The loop starts with the calculation of $\Delta\alpha$ and $\Delta\beta$ for each section. Then the local α and β are obtained by adding the rigid (geometric) value to the flexible results of Eq. (6) and (7). These values are updated in each CFD nodes and

the C_p is interpolated from aerodynamic database. By integrating the pressure field, we obtain the forces and, using the structural solver, deformations are updated. The loop continues whereas a stopping criteria is not satisfied: CFD residual lower than 10^{-5} and CSM displacement variation between iterations less than 1 mm. Next, some consideration about the integration scheme and the interpolation method are discussed.

1. Integration of C_p

When working with a flexible wing, substantial differences are expected between initial and final shapes. The difference between both is the displacement. In Fig. 11a both forms are presented. In blue, the undeformed initial shape; in red, the deformed one.

In this work, the geometric linear effect in Table 1 is the nonlinear treatment considered (see Fig. 11b): the wing modifies its nominal dimensions in order to fit with the exact structural deformations maintaining the same effective wingspan. Despite it is not completely physically correct, it offers a great improvement to the method in terms of accuracy without affecting the robustness. This approach is correct since the maximum deformations are near the limit of 10% semi wingspan specified in Table 1.

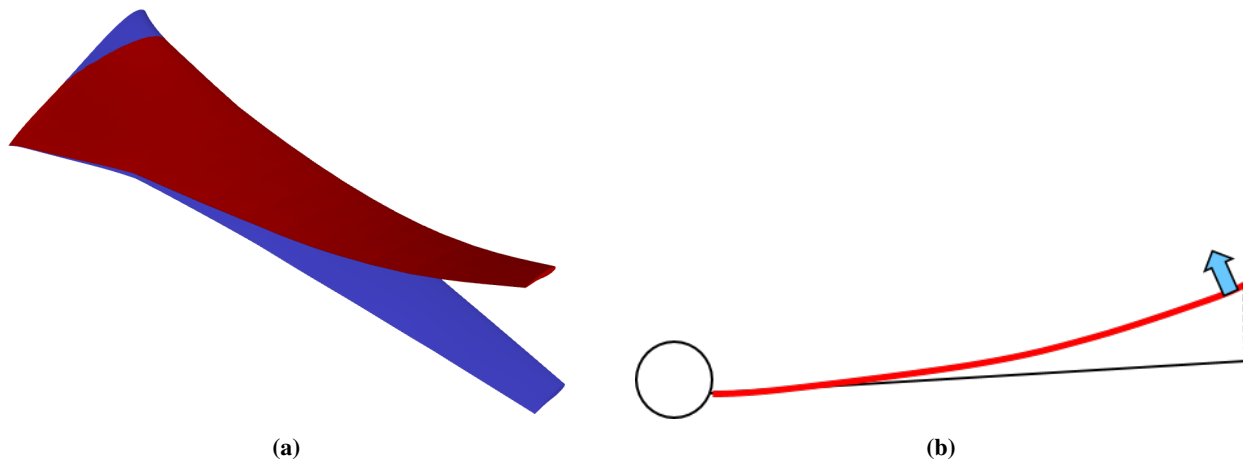


Fig. 11 Nonlinear treatment of the wing for the C_p integration. (a) Wing deformation due to fluid-structure interaction: in blue, the undeformed shape; in red, the deformed one, (b) Geometric linear effect (see Table 1).

2. Interpolation of C_p

Normally, data are not available for the continuous range of incidences and Mach numbers. In the case of aerodynamic nonlinearities, since the stall can happen suddenly, the separation of reliable data in critical zones can worsen the global performance of the method. In the solution presented, a linear approach is used to manage this jump in AoA and Mach regimes.

V. Results

A. Results for transonic regime

The study case is the XRF1 High Aspect Ratio Wing flying at cruise regime ($M = 0.83$). The VLM mesh used in the study is discretized by 40 spanwise sections (N_s) and 16 cells chordwise. In order to validate the capacity of the method to capture the aerodynamics nonlinear effects in a flexible wing aircraft, the input of the our case is recovered from the high-fidelity CFD/CSM (R_y and R_z).

The first consideration tested has been whether the new structural treatment of integrating the C_p through the deformed shape improves the results, presented in Fig. 12. A comparison it is done between two FNSA (one integrating through the deformed shape and the other through the rigid shape *nonGeo FNSA*), the high-fidelity CFD/CSM results and the CFD rigid results. It is observed that the flexible values are lower than the rigid ones, with also lower lift gradient. The new integration yields to better results. Besides, the difference in aerodynamics between the rigid and the flexible wing (above-mentioned in Fig. 4) is also seen here since the stall in the flexible curve is delayed. This effect also derives to a load alleviation in the whole range of incidences treated.

The performance of the FNSA integrating through the deformed shape yields to a maximum error on lift of 6.53%, 9.85% on momentum and 0.008 drag units on C_d . Particularly, until $\alpha = 3^\circ$, the proposed method achieves a perfect fit on lift. However, the pitching moment coefficient is misfit, and an analysis is presented later.

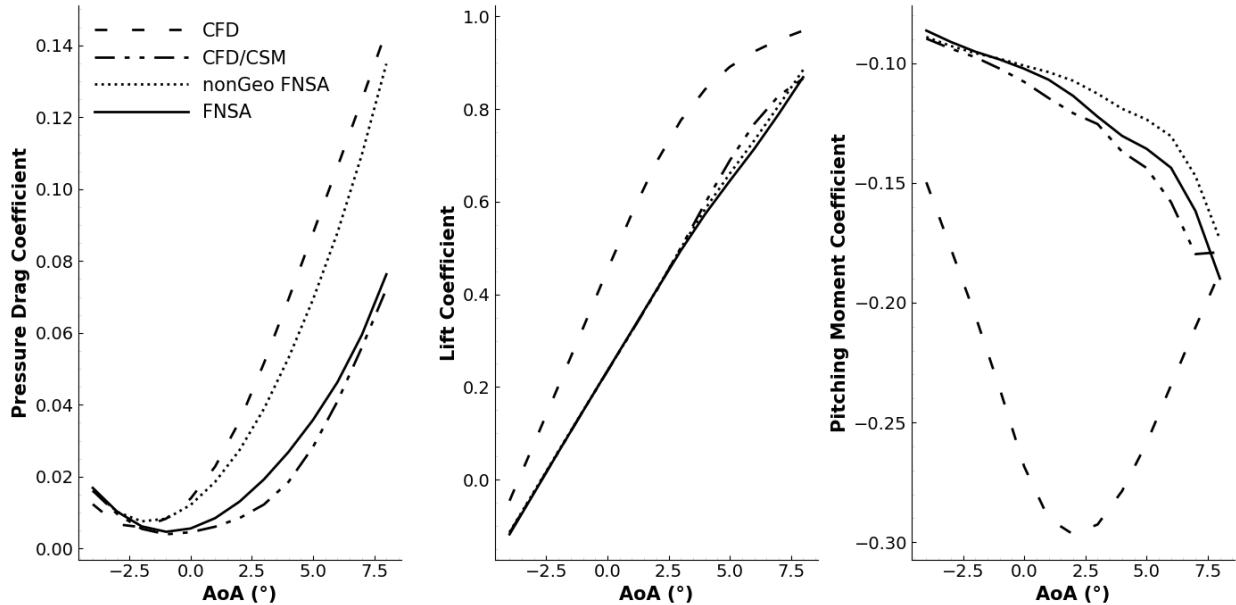


Fig. 12 Polars for cruise Mach, comparing the FNSA results to CFD/CSM and CFD solutions.

The extension presented in this work works with pressure. Thus, the C_p resulting from the fast method process is

compared with the one resulting from the CFD/CSM methodology. In Fig. 13, the results for $AoA = -3^\circ$ are presented; in Fig. 14, for $\alpha = 2^\circ$ and; in Fig. 15, for $\alpha = 7^\circ$.

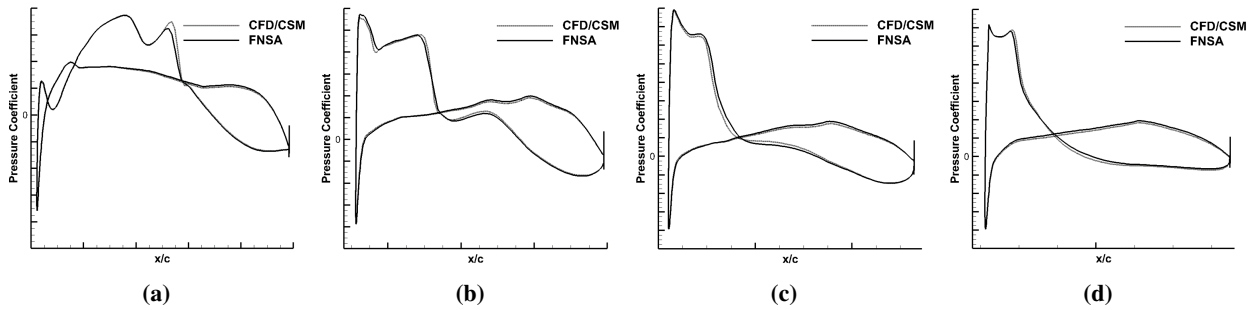


Fig. 13 Comparison of C_p resulting of the FNSA and CFD/CSM solution for $M = 0.83$ at $AoA = -3^\circ$. (a) $\eta = 0.16$, (b) $\eta = 0.38$, (c) $\eta = 0.63$ and, (d) $\eta = 0.95$.

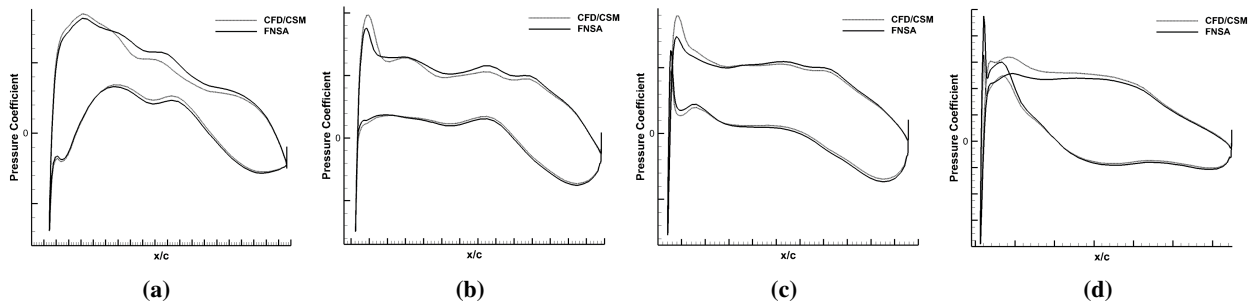


Fig. 14 Comparison of C_p resulting of the FNSA and CFD/CSM solution for $M = 0.83$ at $AoA = 2^\circ$. (a) $\eta = 0.16$, (b) $\eta = 0.38$, (c) $\eta = 0.63$ and, (d) $\eta = 0.95$.

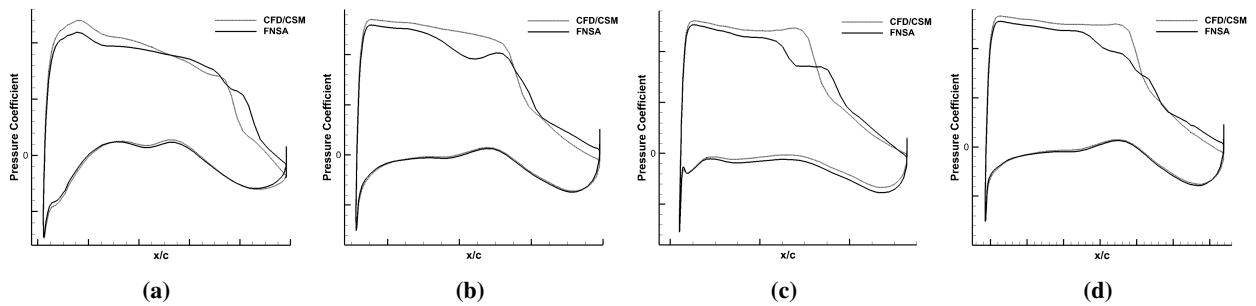


Fig. 15 Comparison of C_p resulting of the FNSA and CFD/CSM solution for $M = 0.83$ at $AoA = 7^\circ$. (a) $\eta = 0.16$, (b) $\eta = 0.38$, (c) $\eta = 0.63$ and, (d) $\eta = 0.95$.

When comparing the pressure distributions at different wingspan positions and different angles of attack it is seen that the method fits the high-fidelity solution. FNSA has the most difficulties at the highest AoA (see Fig. 15), but even in this conditions aligns with CFD/CSM. These C_p plots are similar to the plots presented in Fig. 23-24 by Grozdanov et al. [25] for a near-stall incidence. Figures 13 and 14 confirms the capacities of the method when the pressure field is not fully developed.

Addressing the errors in the momentum plot, considering the expression in Eq. (10), since the deformed shape is directly recovered from the CFD/CSM analysis (isodeformation study), it cannot exist an error derived from the lever arm definition (D_x and D_z). Hence, the only possible source of error are the force terms (F_x and F_z). These terms come from the integration of the pressure field, that in turn is interpolated within the lookup tables. Thus, the source of error could be the interpolation method which is linear here.

$$M = F_x \cdot D_z - F_z \cdot D_x \quad (10)$$

Another source of error could be the unappropriated use the $\Delta\alpha$ and $\Delta\beta$ computed using a lift approach. Indeed, following a similar approach to the one that allows us to define $\Delta\alpha$ from a lift curve, it is possible to get an equivalent gap based on the pitching moment coefficient curve. Since the two values are not the same, the result is necessarily different.

B. Results forcing Mach interpolation

As it has been mentioned in the Section IV, it is possible to face a case demanding an AoA or a Mach regime not present in the database. When running the FNSA in these cases, an interpolation is done. Hence, to evaluate the capacity of the method, the solutions for $M = 0.83$ using lookup tables without the cruise regime data within are tested. The results are presented in Fig. 16.

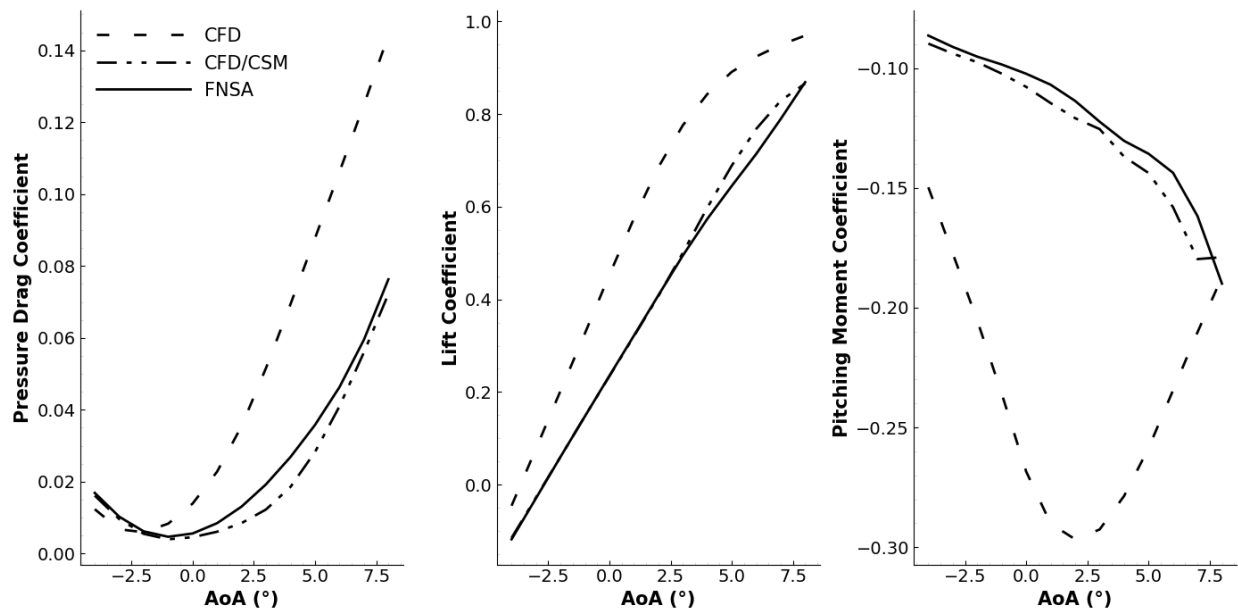


Fig. 16 Polars for cruise Mach, comparing the FNSA results to CFD/CSM and CFD solutions. The look-up tables used have no CFD data for $M = 0.83$.

The performance of the FNSA interpolating in Mach yields to a maximum error on lift of 7%, 10% on momentum and 0.0083 drag units on C_d . The errors presented are really similar to the case of $M = 0.83$ in the lookup tables. These small differences can be explained due to the fact that even if the cruise Mach is not included, near Machs with similar physic behaviors are (i.e. $M = 0.80$ and $M = 0.85$).

C. Results for winglet configuration

As it has been presented in section IV, the formulation naturally adapts to different geometries of the wing. In order to test this feature, pressure fields are presented in Fig. 17 for different incidences at the XRF1 HARW winglet section.

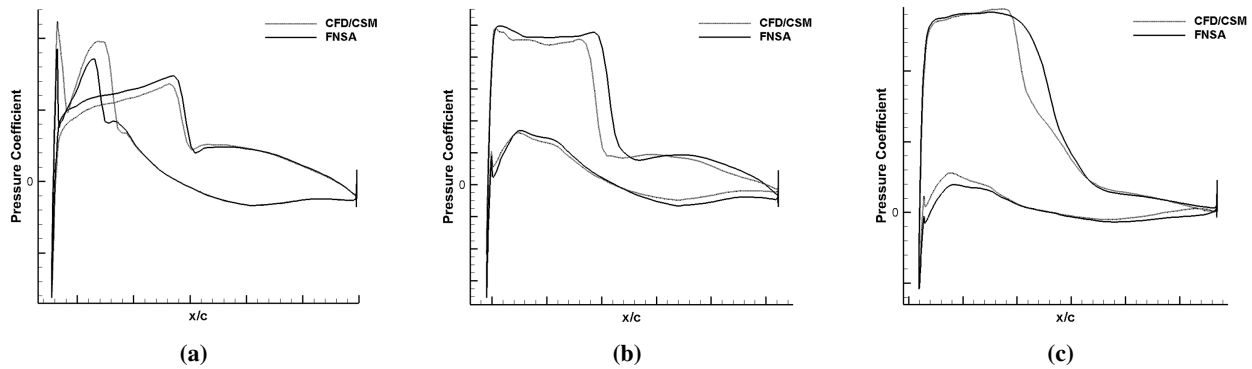


Fig. 17 C_p profiles of the winglet section for different incidences: (a) $\alpha = -3^\circ$, (b) $\alpha = 2^\circ$ and, (c) $\alpha = 7^\circ$. The results of FNSA and CFD/CSM are compared for $M = 0.83$.

Accurate C_p fields are recovered for the winglet section at different incidences. The difference between curves at various incidences is in concordance with the outer section results for the wing case. As we increase the cant angle the pressure differential between upper and lower surfaces of the wing is reduced. The latest occurs because the winglet represents an obstacle to the fluid circulation at the wingtip. If the winglet is well design, its resultant force is decomposed to a inner lift and a forward lift. In consequence, it exists a drag reduction but also a maximum lift devaluation and a modification of the lift slope [40].

D. Results for different Mach regimes

The challenge in high subsonic and transonic computations lies in capturing the correct position where the shocks occur since it is not fixed. In order to illustrate the capabilities of FNSA, four regimes are presented in Fig. 18. Beginning at a low subsonic regime ($M = 0.30$) and finishing at transonic $M = 0.85$ verifies that the biggest differences are done at the transonic regime. In fact, variations grow with the Mach for both C_d (maximum error of 0.007 drag units corresponding to $M = 0.85$) yielding to more important deviations in C_m (with the of 13.54% at $M = 0.85$). For the pitching moment, it is also observed a change in the trend at the time that the transonic regime is analyzed: for subsonic Mach numbers, the moment gradients were becoming less negative with similar behaviors but, a sudden fall is observed for the transonic Mach number. The errors committed in lift are almost null at the lowest Mach (2%) and it

augments until an error of 6% for the transonic regime. It is observed that the lift slope slightly varies ($\partial C_l / \partial \alpha = 0.075$ for $M = 0.30$ to $\partial C_l / \partial \alpha = 0.087$ for $M = 0.85$).

Finally, the compressibility correction gives satisfactory results in the studied cases, but the importance of a high quality database is sensed from high AoA for transonic Mach.

These results improve those presented by Skujins et al. [28] in section VII of their article.

E. Sensibility to VLM mesh

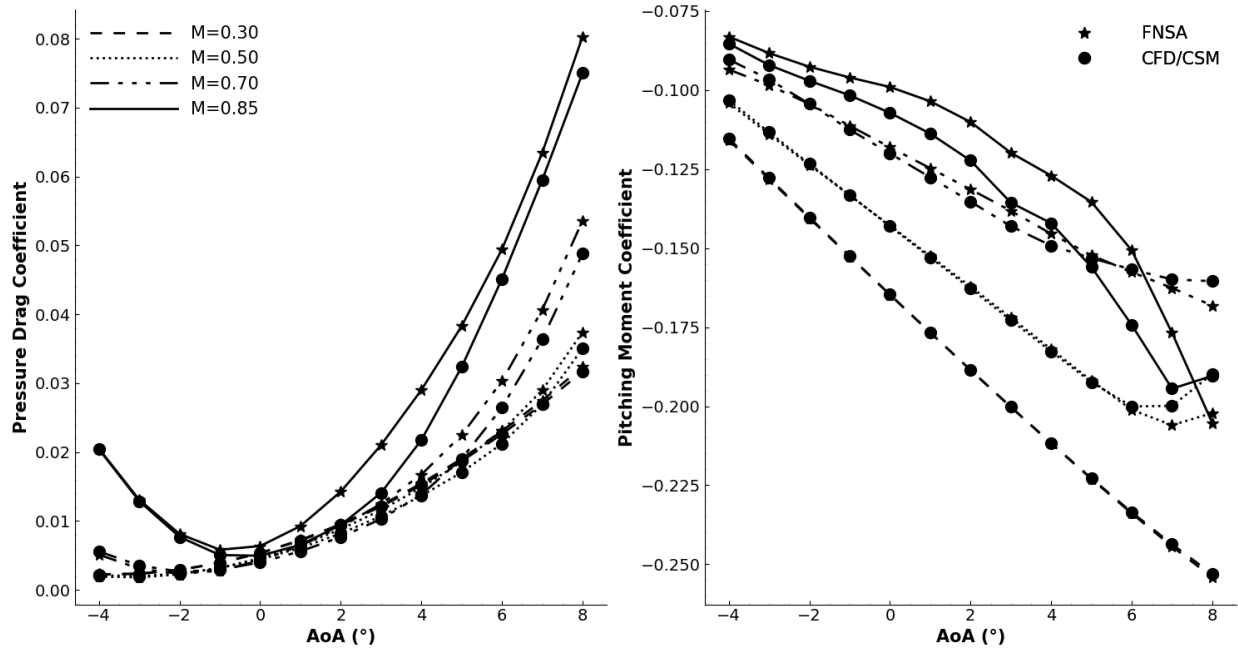
Whereas the quality of the lookup tables drives the robustness of the method, in this section we wonder about the influence of AIC matrices size. Since it uses the variation of incidence and sideslip to recover the information stored in the lookup tables, the VLM mesh used to compute the AIC matrices is a keystone (the higher the number of sections, the smoother the flexible response of the method). Figure 19 shows the influence of N_s value to FNSA performance. The results show the capacity of the method to give accurate solutions with independence to the VLM discretization. This is interesting in order to work with smaller matrices. For instance, the size of a VLM matrix varies from 1.85 kB for $N_s = 20$ to 6.82 kB for $N_s = 80$. As a VLM matrix is stored for each Mach and for both α and β , an memory economy of 59.64 kB could be achieved when considering 6 Mach regimes. The difference in time employed for VLM matrices construction and for solving the FNSA can be neglected.

VI. Conclusions

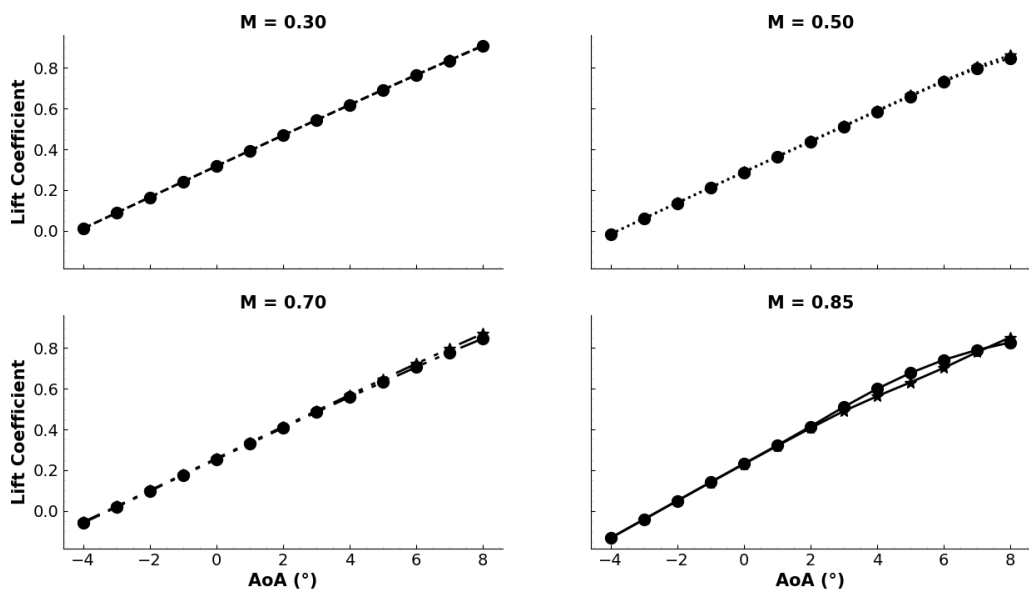
This work shows the capacity of the flexible FNSA to compute aeroelastic loads capturing the transonic aerodynamic nonlinearities due to compressibility and viscosity. The speed and accuracy performance of the FNSA are largely acceptable for loads computation. Besides, the current methodology is found to be versatile and very robust. Using a pre-computed database containing the 3D nonlinear local polars, problems of convergence and mesh deformation are avoided. Particularly, this database can be filled with computational solutions obtained with high-fidelity solvers, but also with experimental data from WTT or flight test campaigns.

Besides, one of the objectives of this work was to show the robustness of the fast method. The good results obtained from the different Mach regimes and the sensibility study to the VLM mesh ensure the goal. In particular these results yield to three comments:

- The competence of the method to treat any Mach regimes is achieved thanks to the capacity to capture the nonlinear effects, heritage of the lookup tables data.
- Despite the fact that the accuracy of the method depends –basically– on the fidelity of the data stored within the lookup tables, the method offers always a result for the case studied.
- The quality of the VLM mesh does not affect the accuracy of the results.



(a)
 ★ FNSA ● CFD/CSM



(b)

Fig. 18 Polars for the wing at four Mach numbers, comparing the FNSA results to CFD/CSM solutions. (a) drag and pitching moment coefficients, (b) lift coefficient.

The proposed methodology also allows less pre-processing compared to the high-fidelity alternatives –such as meshing effort or convergence tests. Once the database is created, the aerodynamics properties are computed in one

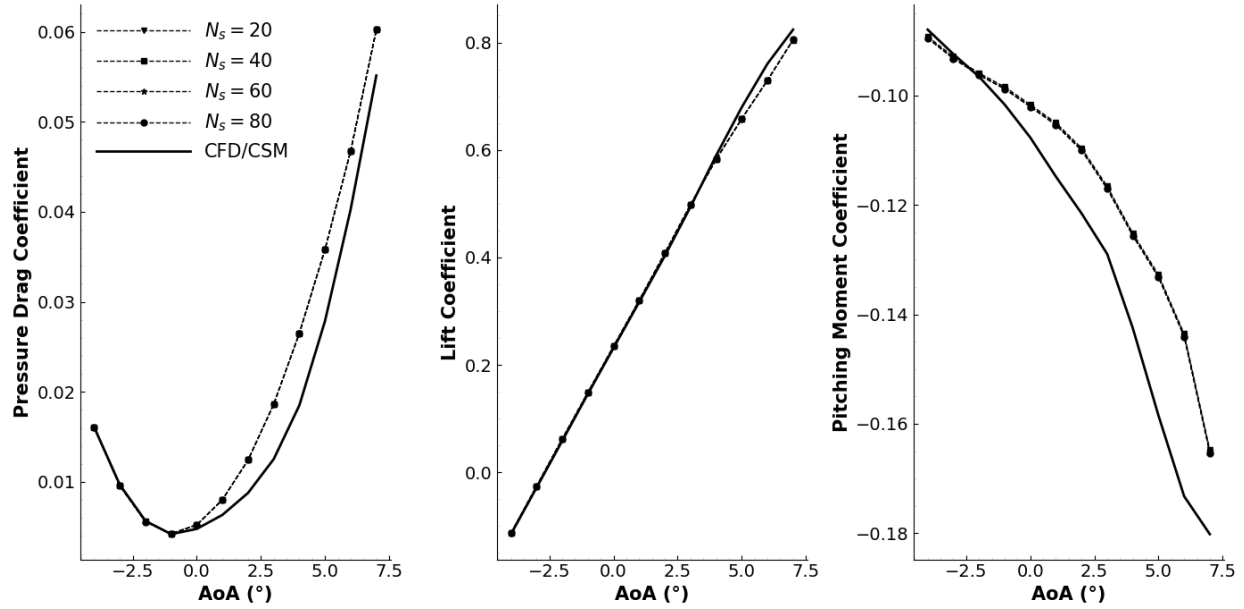


Fig. 19 Comparison of polar curves when flying at $M = 0.83$ between FNSA results for four different VLM discretizations, and the CFD/CSM solution.

second; compared to the mean time of $7h30'$ for single CFD simulation (one AoA at a specific Mach number). This considerable difference in computation time offers an interesting advantage when facing a pre-design problem or an optimisation process taking into account different disciplines.

The methodology uses the linear deformed shape of the wing to integrate the pressure field. This implementation gives interesting results for the drag estimation coefficient. Thus, also the accuracy in computing the pitching moment coefficient improves. Integrating with respect to the linear elastic deformed shape (even without being completely physically appropriate) is an option to consider the effect of the wing dihedral change. This feature permits to deliver more accurate loads.

Furthermore, known the complexity of shocks, in particular in the transonic region where they are not fixed, implementing a linear interpolation method limits its degree of freedom to approximate the fluid discontinuities. Noticing that interpolating within α yields to worst results than when deducting the value from other Mach numbers data, we could prioritize interpolating in M when information is missing. This procedure could yield to a data fusion strategy (i.e. combining α and M).

Also cutting-edge methods such as nonlinear interpolation algorithms, machine learning or surrogate methods, among others, could be used to recover the data from the lookup tables, offering better performance and committing a smaller numerical error whereas interpolating.

Finally, the methodology models with no difficulty different wings configurations: winglets, sweep and dihedral. If data are available, we need to create the correspondent VLM mesh and condensed stiffness model and correlate them to the data. This has been tested in a winglet configurations achieving accurate results.

Acknowledgments

An Acknowledgments section, if used, **immediately precedes** the References. Sponsorship information and funding data are included here. The preferred spelling of the word “acknowledgment” in American English is without the “e” after the “g.” Avoid expressions such as “One of us (S.B.A.) would like to thank. . .” Instead, write “F. A. Author thanks. . .” Sponsor and financial support acknowledgments are also to be listed in the “acknowledgments” section.

References

- [1] Voglsinger, M., and Perez-Sanchez, J., “Wing, in particular airfoil of an aircraft, with a variable profile shape,” *US Patent 7918421B2*, 2011.
- [2] Pendleton, E., Flick, P., Paul, D., Voracek, D., Reichenbach, E., and Griffin, K., “The X-53 A Summary of the Active Aeroelastic Wing Flight Research Program,” *AIAA Structures, Structural Dynamics, and Materials Conference*, 2007. <https://doi.org/10.2514/6.2007-1855>.
- [3] Wood, N., “Morphing Aerofoil,” *US Patent 9745048B2*, 2017.
- [4] Ashley, S., “Flying on Flexible Wings,” *Scientific American*, Vol. 289, No. 5, 2003, pp. 84–91.
- [5] Cook, R., Palacios, R., and Goulart, P., “Robust Gust Alleviation and Stabilization of Very Flexible Aircraft,” *AIAA Journal*, Vol. 51, No. 2, 2013, pp. 330–340. <https://doi.org/10.2514/1.J051697>.
- [6] Volk, J., “Control System for Alleviating a Gust Load on an Aircraft Wing,” *US Patent 6766981B2*, 2004.
- [7] Jasa, J. P., Hwang, J. T., and Martins, J. R. R. A., “Open-source coupled aerostructural optimization using Python,” *Structural and Multidisciplinary Optimization*, Vol. 57, No. 4, 2018, pp. 1815–1827. <https://doi.org/10.1007/s00158-018-1912-8>.
- [8] Gray, J. S., Hwang, J. T., Martins, J. R. R. A., Moore, K. T., and Naylor, B. A., “OpenMDAO: An open-source framework for multidisciplinary design, analysis, and optimization,” *Structural and Multidisciplinary Optimization*, Vol. 59, No. 4, 2019, pp. 1075–1104. <https://doi.org/10.1007/s00158-019-02211-z>.
- [9] Martins, J. R. R. A., and Lambe, A. B., “Multidisciplinary Design Optimization: A Survey of Architectures,” *AIAA Journal*, Vol. 51, No. 9, 2013, pp. 2049–2075. <https://doi.org/10.2514/1.J051895>.
- [10] Guenov, M. D., and Kessler, E., *Advances in Collaborative Civil Aeronautical Multidisciplinary Design Optimization*, American Institute of Aeronautics and Astronautics, Inc., Virginia, 2010.

- [11] Hansen, L. U., Heinze, W., and Horst, P., “Blended wing body structures in multidisciplinary pre-design,” *Struct Multidisc Optim*, , No. 36, 2008, pp. 93–106. <https://doi.org/10.1007/s00158-007-0161-z>.
- [12] Guenov, M., Fantini, P., Balachandran, L., Maginot, J., Padulo, M., and Nunez, M., “Multidisciplinary Design Optimization Framework for the Pre Design Stage,” *J Intell Robot Syst*, , No. 59, 2010, pp. 223–240. <https://doi.org/10.1007/s10846-010-9397-8>.
- [13] Ronch, A. D., “Special Issue: Aeroelasticity,” *Aerospace*, Vol. 6, No. 92, 2019. <https://doi.org/10.3390/aerospace6090092>.
- [14] Wright, J., and Cooper, J., *Introduction to Aircraft Aeroelasticity and Loads*, American Institute of Aeronautics and Astronautics, Inc., Washington, DC, 2007.
- [15] Fernandez-Escudero, C., Gagnon, M., Laurendeau, E., Prothin, S., Michon, G., and Ross, A., “Comparison of low, medium and high fidelity numerical methods for unsteady aerodynamics and nonlinear aeroelasticity,” *Journal of Fluids and Structures*, Vol. 91, No. 102744, 2019. <https://doi.org/10.1016/j.jfluidstructs.2019.102744>.
- [16] Dang, H., Yang, Z., and Li, Y., “Accelerated loosely-coupled CFD/CSD method for nonlinear static aeroelasticity analysis,” *Aerospace Science and Technology*, Vol. 14, No. 4, 2010, pp. 250–258. <https://doi.org/10.1016/j.ast.2010.01.004>.
- [17] Crovato, A., Almeida, H. S., Vio, G., Silva, G. H., Prado, A. P., Breviglieri, C., Guner, H., Cabral, P. H., Boman, R., Terrapon, V. E., and Dimitriadis, G., “Effect of Levels of Fidelity on Steady Aerodynamic and Static Aeroelastic Computations,” *Aerospace*, Vol. 7, No. 42, 2020. <https://doi.org/10.3390/aerospace7040042>.
- [18] Anderson, J. D., *Fundamentals of aerodynamics*, McGraw-Hill, New York, NY, 2001.
- [19] Carrella, A., and Elvins, D. J., “Identifying and quantifying structural nonlinearities in engineering applications from measured frequency response functions,” *Mechanical Systems and Signal Processing*, Vol. 25, No. 3, 2011, pp. 1011–1027. <https://doi.org/10.1016/j.ymssp.2010.09.011>.
- [20] Miranda, L. R., Elliot, R. D., and Baker, W. M., “A Generalized Vortex Lattice Method for Subsonic and Supersonic Flow Applications,” *NASA Contractor*, , No. Report 2865, 1977.
- [21] Guermond, J.-L., “A generalized lifting-line theory for curved and swept wings,” *Journal of Fluid Mechanics*, Vol. 211, 1990, pp. 497–513. <https://doi.org/10.1017/S0022112090001665>.
- [22] Fung, Y. C., *An introduction to the theory of aeroelasticity*, Dover Publications, Inc., Phoenix, 1993.
- [23] Katz, J., and Plotkin, A., *Low-Speed Aerodynamics*, Cambridge University Press, Cambridge, 2001.
- [24] Agostinelli, C., Allen, C., and Rampurawal, A., “Flexible Wing Twist Optimisation using Rapid Computational Methods,” *30th AIAA Applied Aerodynamics Conference*, 2012. <https://doi.org/10.2514/6.2012-2661>.
- [25] Grozdanov, A., and Laurendeau, E., “Transonic Aeroelasticity using the 2.5D non-linear vortex-lattice method,” *IFASD*, 2017.

- [26] Goitia, H., and Llamas, R., “Nonlinear Vortex Lattice Method for Stall Prediction,” *MATEC Web Conf.*, Vol. 304, No. 02006, 2019. <https://doi.org/10.1051/mateconf/201930402006>.
- [27] Kontogiannis, A., Parenteau, M., and Laurendeau, E., “Viscous-Inviscid Analysis of Transonic Swept Wings using 2.5D RANS and Parametric Shapes,” *AIAA SciTech*, 2019. <https://doi.org/10.2514/6.2019-2116>.
- [28] Skujins, T., and Cesnik, C. E. S., “Reduced-Order Modeling of Unsteady Aerodynamics Across Multiple Mach Regimes,” *Journal of Aircraft*, Vol. 51, No. 6, 2014, pp. 1681–1704. <https://doi.org/10.2514/1.C032222>.
- [29] Bekemeyer, P., Ripepi, M., Heinrich, R., and Görtz, S., “Nonlinear Unsteady Reduced-Order Modeling for Gust-Load Predictions,” *AIAA Journal*, Vol. 57, No. 5, 2019, pp. 1839–1850. <https://doi.org/10.2514/1.J057804>.
- [30] Rule, J. A., Cox, D. E., and Clark, R. L., “Aerodynamic Model Reduction Through Balanced Realization,” *AIAA Journal Technical Notes*, Vol. 42, No. 5, 2004, pp. 1045–1858. <https://doi.org/10.2514/1.9596>.
- [31] Barriety, B., Boin, J.-P., Chandre-Vila, O., and Mauermann, T., “Fast Fluid-Structure Computational Method Taking into Account Non-linear Aerodynamic,” *IFASD*, 2019.
- [32] Riso, C., Sanghi, D., Cesnik, C., Vetrano, F., and Teufel, P., “Parametric Roll Maneuverability Analysis of a High-Aspect-Ratio-Wing Civil Transport Aircraft,” *AIAA Scitech Forum*, , No. 1191, 2020. <https://doi.org/10.2514/6.2020-1191>.
- [33] Sanghi, D., Riso, C., Cesnik, C., and Vetrano, F., “Influence of Aileron Placement on Roll Response of High-Aspect-Ratio-Wing Aircraft,” *AIAA Aviation Forum*, , No. 2645, 2020. <https://doi.org/10.2514/6.2020-2645>.
- [34] MSC Software, *Nastran 2012.2 Quick Reference Guide*, 2012.
- [35] DLR, *TAU-code User Guide*, 2016.
- [36] Spalart, P. R., and Allmaras, S. R., “A One-Equation Turbulence Model for Aerodynamic Flows,” *Recherche Aerospatiale*, , No. 1, 1994, pp. 5–21. <https://doi.org/10.2514/6.1992-439>.
- [37] Wilcox, D. C., “Formulation of the k-w Turbulence Model Revisited,” *AIAA Journal*, Vol. 46, No. 11, 2008, pp. 2823–2838. <https://doi.org/10.2514/1.36541>.
- [38] Gibson, M. M., and Rodi, W., “A Reynolds-stress closure model of turbulence applied to the calculation of a highly curved mixing layer,” *Journal of Fluid Mechanics*, Vol. 103, 1981, pp. 161–182. <https://doi.org/10.1017/S0022112081001286>.
- [39] Glauert, H., “The effect of compressibility on the lift of an aerofoil,” *Proceedings of the Royal Society A: Mathematical, Physical and Engineering Sciences*, Vol. 118, No. 779, 1928, pp. 113–119. <https://doi.org/10.1098/rspa.1928.0039>.
- [40] Guerrero, J., Sanguineti, M., and Wittkowski, K., “CFD Study of the Impact of Variable Cant Angle Winglets on Total Drag Reduction,” *Aerospace*, Vol. 5, No. 126, 2018. <https://doi.org/10.3390/aerospace5040126>.